

Statistical connection of peak counts to power spectrum and moments in weak lensing field

Masato Shirasaki^{*},

Division of Theoretical Astronomy, National Astronomical Observatory of Japan, 2-21-1 Osawa, Mitaka, Tokyo 181-8588, Japan

Accepted XXX. Received YYY; in original form 3/3/2016

ABSTRACT

The number density of local maxima of weak lensing field, referred to as weak-lensing peak counts, can be used as a cosmological probe. However, its relevant cosmological information is still unclear. We study the relationship between the peak counts and other statistics in weak lensing field by using 1000 ray-tracing simulations. We construct a local transformation of lensing field \mathcal{K} to a new Gaussian field y , named local-Gaussianized transformation. We calibrate the transformation with numerical simulations so that the one-point distribution and the power spectrum of \mathcal{K} can be reproduced from a single Gaussian field y and monotonic relation between y and \mathcal{K} . Therefore, the correct information of two-point clustering and any order of moments in weak lensing field should be preserved under local-Gaussianized transformation. We then examine if local-Gaussianized transformation can predict weak-lensing peak counts in simulations. The local-Gaussianized transformation is insufficient to explain weak-lensing peak counts in the absence of shape noise. The prediction by local-Gaussianized transformation underestimates the simulated peak counts with a level of $\sim 20 - 30\%$ over a wide range of peak heights. Local-Gaussianized transformation can predict the weak-lensing peak counts with a $\sim 10\%$ accuracy in the presence of shape noise. Our analyses suggest that the cosmological information beyond power spectrum and its moments would be necessary to predict the weak-lensing peak counts with a percent-level accuracy, which is an expected statistical uncertainty in upcoming wide-field galaxy surveys.

Key words: gravitational lensing: weak, large-scale structure of Universe

1 INTRODUCTION

Gravitational lensing is caused by bending of the light emitted from a distant source, which is a prediction by General Relativity. Since the exact amount of bending depends on projected mass along a line of sight, gravitational lensing is now recognised as direct and very promising probe of the matter distribution in the Universe. In general, foreground matter causes small distortions of the images of distant background galaxies, and these small distortions contain rich information on the foreground matter distribution and its growth over time, which are sensitive to the nature of dark energy and dark matter (e.g., [Huterer 2010](#); [Kilbinger 2015](#), for a review). In order to extract cosmological information from image distortion induced by gravitational lensing, various statistical methods have been proposed in the literature. Mapping matter distribution on a continuous sky is a key, basic method among them (e.g., [Massey et al. 2007](#); [Van Waerbeke et al. 2013](#); [Chang et al. 2015](#)). Non-Gaussian features in the reconstructed density field are produced by non-linear gravitational growth and can not be extracted by means of the conventional statistics of cosmic shear such as two-point correlation function or power spectrum (e.g., [Pen et al. 2003](#)).

The statistics of local maxima found in a reconstructed lensing map have cosmological information originated from massive dark matter haloes. The height of peaks are commonly normalised by the noise variance of a reconstructed map σ . The local maxima with the height of $\gtrsim 3\sigma$ significance are expected to be caused by high density regions in the Universe that correspond to massive collapsed objects such as clusters of galaxies (e.g., [Hamana et al. 2004](#); [Hennawi & Spergel 2005](#); [Maturi et al. 2005](#); [Marian et al. 2012](#); [Hamana et al. 2012](#)). The one-to-one correspondence between clusters and lensing peaks has been confirmed by recent galaxy imaging surveys (e.g., [Miyazaki et al. 2007](#); [Schirmer et al. 2007](#); [Shan et al. 2012](#); [Miyazaki et al. 2015](#)). Therefore, the number count of high-significance peaks can be associated with the abundance of galaxy clusters that is highly sensitive to growth of matter density perturbations (e.g., [Lilje 1992](#)). The peak counts can be used to place interesting constraints on the matter density perturbation in the Universe (e.g., [Marian & Bernstein 2006](#); [Dietrich & Hartlap 2010](#)), the nature of dark energy (e.g., [Marian et al. 2011](#)), the statistical property of initial density perturbations (e.g., [Hilbert et al. 2012](#)) and the modification of General Relativity (e.g., [Shirasaki et al. 2016](#)). Several observational constraints also have been obtained in the recent lensing surveys (e.g., [Liu et al. 2015b](#); [Hamana et al. 2015](#); [Liu et al. 2016](#)).

^{*} E-mail: masato.shirasaki@nao.ac.jp

Numerical simulations suggest that cosmological information in the number density of lensing peaks can be carried by not only high-significance peaks but also the peaks with $\sim 1 - 2\sigma$ significance (Kratovichil et al. 2010). We call such peaks with intermediate height as medium peaks. There exist observational studies to constrain on cosmological models by counting medium peaks (e.g., Liu et al. 2015a; Kacprzak et al. 2016). Since the medium peaks have similar heights to the noise variance by definition, it is not straightforward to infer their relevant cosmological information. Fisher analyses with a large set of numerical simulations clearly show that counting medium peaks can improve the cosmological constraints by weak-lensing power spectrum alone (Bard et al. 2013). The improvement of cosmological constraints by weak-lensing peak counts has been demonstrated with actual data (Liu et al. 2015a). Thus, medium peaks are expected to contain non-Gaussian information but it is uncertain which levels of non-Gaussianity are important. Detailed comparisons between the angular position of medium peaks and dark matter halos along a line of sight show that medium peaks can be generated by superposition of large-scale structures and multiple dark matter halos, whereas the intrinsic ellipticities of sources can further compromise the correlation between medium peaks and dark matter halos (Yang et al. 2011). Liu & Haiman (2016) perform similar analysis with actual data set to show the angular correlation of medium peaks with galaxies on sky, suggesting that the origin of medium peaks can not be explained by observational noise alone. The number count of medium peaks is also found to be insensitive to the internal structure of dark matter halos (Yang et al. 2013) and the details of baryonic physics (Osato et al. 2015). Although halo-based approaches have been developed to predict the peak counts over a wide range of peak heights (e.g. Lin & Kilbinger 2015; Zorrilla Matilla et al. 2016), it is still insufficient to make a prediction with a few percent accuracy, corresponding to the statistical uncertainty in upcoming lensing surveys.

To infer the cosmological information in weak-lensing peak counts, we study the relation of cosmological information in weak-lensing peak counts and other lensing statistics. For comparison, we consider the power spectrum and its moments of weak lensing field. We assume a simple monotonic relation between a reconstructed lensing map and a new Gaussian field, named local-Gaussianized transformation (also see Yu et al. 2016, for the related work). We construct such relationship by a local mapping and calibrate that the one-point probability distribution function (PDF) and the power spectrum of simulated lensing field can be reproduced with a $\sim 5\%$ accuracy. Thus, after calibrations, our model based on local-Gaussianized transformation should include appropriate cosmological information of two-point clustering and moments in calculation of expected peak counts. By comparing such theoretical models and simulated peak counts, we examine if the peak counts can be fully explained by cosmological information of power spectrum and one-point PDF of lensing field.

The paper is organised as follows. In Section 2, we briefly describe the basics of weak gravitational lensing. There, we also introduce a general expression of weak-lensing peak counts and a local transformation of weak lensing field to a Gaussian field. We also summarise our ray-tracing simulations and how to construct a local-Gaussianized transformation from these simulations in Section 3. By using our theoretical model and a large set of ray-tracing simulations, we examine if peak counts can include the cosmological information beyond the two-point clustering and moments in Section 4. Conclusions and discussions are summarised in Section 5.

2 WEAK GRAVITATIONAL LENSING

2.1 Basics

We first summarise the basics of gravitational lensing induced by large-scale structure. Weak gravitational lensing effect is usually characterised by the distortion of image of a source object by the following 2D matrix:

$$A_{ij} = \frac{\partial \beta_i}{\partial \theta_j} \equiv \begin{pmatrix} 1 - \kappa - \gamma_1 & -\gamma_2 \\ -\gamma_2 & 1 - \kappa + \gamma_1 \end{pmatrix}, \quad (1)$$

where we denote the observed position of a source object as θ and the true position as β , κ is the convergence, and γ is the shear. In the weak lensing regime (i.e., $\kappa, \gamma \ll 1$), one can express the weak lensing convergence field as the integral of matter overdensity field $\delta(x)$ along a line of sight (Bartelmann & Schneider 2001),

$$\kappa(\theta, \chi_{\text{source}}) = \frac{3}{2} \left(\frac{H_0}{c} \right)^2 \Omega_{m0} \int_0^\chi d\chi \times \frac{r(\chi_{\text{source}} - \chi)r(\chi)}{r(\chi_{\text{source}})} \frac{\delta[r(\chi)\theta, \chi]}{a(\chi)}, \quad (2)$$

where χ is the comoving distance, χ_{source} is the comoving distance to a source, $r(\chi)$ is the angular diameter distance, H_0 is the present-day Hubble constant and Ω_{m0} represents the matter density parameter at present. Throughout this paper, we assume that source galaxies locate at single plane with the redshift of $z_{\text{source}} = 1$ for simplicity.

Power spectrum

The power spectrum is one of the basic statistics in modern cosmology (e.g., Anderson et al. 2012; Planck Collaboration et al. 2015; Becker et al. 2016). It is defined as the two-point correlation in Fourier space:

$$\langle \tilde{\kappa}(\ell_1) \tilde{\kappa}(\ell_2) \rangle = (2\pi)^2 \delta_D(\ell_1 + \ell_2) P_\kappa(\ell_1), \quad (3)$$

where $\delta_D(x)$ is the Dirac delta function and the multipole ℓ is related to the angular scale through $\theta = \pi/\ell$. By using the Limber approximation (Limber 1954; Kaiser 1992) and Eq. (2), one can express the convergence power spectrum as

$$P_\kappa(\ell) = \int_0^{\chi_{\text{source}}} d\chi \frac{W(\chi)^2}{r(\chi)^2} P_\delta \left(k = \frac{\ell}{r(\chi)}, z(\chi) \right), \quad (4)$$

where $P_\delta(k)$ represents the three dimensional matter power spectrum, and $W(\chi)$ is the lensing weight function defined as

$$W(\chi) = \frac{3}{2} \left(\frac{H_0}{c} \right)^2 \Omega_{m0} \frac{r(\chi_{\text{source}} - \chi)r(\chi)}{r(\chi_{\text{source}})} (1 + z(\chi)). \quad (5)$$

Reconstruction of smoothed convergence

In actual observations, one usually start with the cosmic shear instead of the convergence field. The reconstruction of smoothed convergence is commonly based on the smoothed map of cosmic shear. Let us first define the smoothed convergence map as

$$\mathcal{K}(\theta) = \int d^2\phi \kappa(\theta - \phi) U(\phi), \quad (6)$$

where U is the filter function to be specified below. We can calculate the same quantity by smoothing the shear field γ as

$$\mathcal{K}(\theta) = \int d^2\phi \gamma_+(\phi : \theta) Q_+(\phi), \quad (7)$$

where γ_+ is the tangential component of the shear at position ϕ relative to the point θ . The filter function for the shear field Q_+ is related to U by

$$Q_+(\theta) = \int_0^\theta d\theta' \theta' U(\theta') - U(\theta). \quad (8)$$

We consider a filter function Q_+ that has a finite extent. In such cases, one can write

$$U(\theta) = 2 \int_\theta^{\theta_o} d\theta' \frac{Q_+(\theta')}{\theta'} - Q_+(\theta), \quad (9)$$

where θ_o is the outer boundary of the filter function. Note that the filter function U should be compensated because the smoothed field \mathcal{K} does not depend on undetermined constant (Schneider 1996).

In the following, we consider the truncated Gaussian filter (for U):

$$U(\theta) = \frac{1}{\pi\theta_G^2} \exp\left(-\frac{\theta^2}{\theta_G^2}\right) - \frac{1}{\pi\theta_o^2} \left[1 - \exp\left(-\frac{\theta_o^2}{\theta_G^2}\right)\right], \quad (10)$$

$$Q_+(\theta) = \frac{1}{\pi\theta^2} \left[1 - \left(1 + \frac{\theta^2}{\theta_G^2}\right) \exp\left(-\frac{\theta^2}{\theta_G^2}\right)\right], \quad (11)$$

for $\theta \leq \theta_o$ and $U = Q_+ = 0$ elsewhere. Throughout this paper, we set $\theta_o = 150$ arcmin and study three cases of $\theta_G = 1.2, 2.4$ and 4.8 arcmin. Note that the choice of $\theta_G = 1.2$ arcmin is found to be an optimal smoothing scale for the detection of massive galaxy clusters using weak lensing for $z_{\text{source}} = 1.0$ (Hamana et al. 2004).

2.2 Peak counts

In this paper, we consider the number density of local maxima in smoothed convergence field \mathcal{K} . The number density of extrema is expressed as (Bardeen et al. 1986; Bond & Efstathiou 1987)

$$n_{\text{ext}}(\theta) = \sum_{\text{ext}} \delta_D(\theta - \theta_{\text{ext}}) = |\det \zeta| \delta_D(\eta), \quad (12)$$

where $\eta_i = \nabla_i \mathcal{K}$, $\zeta_{ij} = \nabla_i \nabla_j \mathcal{K}$ and we use the relation that $\eta_i(\theta) = \zeta_{ij}(\theta_j - \theta_{\text{ext},j})$ around the position of extrema θ_{ext} . For a given multiplicative PDF of \mathcal{K} , η and ζ , the expected number density of local maxima with fixed peak height of α can be obtained by

$$\frac{dn_{\text{peak}}}{d\mathcal{K}} \Big|_{\mathcal{K}=\alpha} = \int d\mathbf{D} \text{Prob}(\mathbf{D}) \delta_D(\mathcal{K} - \alpha) |\det \zeta| \times \delta_D(\eta) \mathcal{H}(\lambda), \quad (13)$$

where $\mathbf{D} = \{\mathcal{K}, \eta, \zeta\}$, λ_i represents the eigen value of $-\zeta$ and $\mathcal{H}(x)$ is the heaviside step function.

Eq. (13) is a general expression of the number density of local maxima for a given two-dimensional field. It is more useful to decompose the observed \mathcal{K} field into two contributions;

$$\mathcal{K} = \mathcal{K}_{\text{cosmo}} + \mathcal{N}, \quad (14)$$

where $\mathcal{K}_{\text{cosmo}}$ represents the cosmological convergence from large-scale structure in the Universe and \mathcal{N} is the noise convergence coming from intrinsic ellipticity of source galaxies known as shape noise. On the assumption that the intrinsic ellipticities of two distant galaxies are uncorrelated each other, the statistical property of \mathcal{N} should be characterised by a Gaussian distribution. Then, the PDF of $\mathbf{D}_N = \{\mathcal{N}, \eta_N, \zeta_N\}$ is given by

$$\text{Prob}(\mathbf{D}_N) = \frac{1}{(2\pi)^3 \sqrt{\det \mathbf{M}_N}} \exp\left(-\frac{1}{2} \mathbf{D}_N^T \mathbf{M}_N^{-1} \mathbf{D}_N\right), \quad (15)$$

where \mathbf{M}_N is the correlation matrix of noise field. The correlation matrix \mathbf{M}_N takes the following forms:

$$\langle \mathcal{N} \mathcal{N} \rangle = \sigma_{\mathcal{N}0}^2, \quad (16)$$

$$\langle \mathcal{N} \eta_{N,i} \rangle = 0, \quad (17)$$

$$\langle \mathcal{N} \zeta_{N,ij} \rangle = -\frac{1}{2} \sigma_{\mathcal{N}1}^2 \delta_{ij}, \quad (18)$$

$$\langle \eta_{N,i} \eta_{N,j} \rangle = \frac{1}{2} \sigma_{\mathcal{N}1}^2 \delta_{ij}, \quad (19)$$

$$\langle \eta_{N,i} \zeta_{N,jk} \rangle = 0, \quad (20)$$

$$\langle \zeta_{N,ij} \zeta_{N,kl} \rangle = \frac{1}{8} \sigma_{\mathcal{N}2}^2 (\delta_{ij} \delta_{kl} + \delta_{ik} \delta_{jl} + \delta_{il} \delta_{jk}), \quad (21)$$

where $\sigma_{\mathcal{N}i}^2$ represents the i -th moment of \mathcal{N} . It is calculated from the power spectrum of \mathcal{N} as follows (van Waerbeke 2000);

$$\sigma_{\mathcal{N}i}^2 = \frac{\sigma_e^2}{2n_{\text{gal}}} \int_0^\infty \frac{d^2 \ell}{(2\pi)^2} \ell^{2i} |\tilde{U}(\ell)|^2, \quad (22)$$

where σ_e is the rms value of the intrinsic ellipticity of the source galaxies, n_{gal} is the number density of galaxies, and $\tilde{U}(\ell)$ represents the Fourier transform of Eq. (10). When θ_o is set to be 150 arcmin in Eq. (10), the functional form of $|\tilde{U}(\ell)|^2$ can be approximated as

$$|\tilde{U}(\ell)|^2 = \exp\left[-\frac{1}{2} \left(\frac{\ell}{\ell_G}\right)^2\right] + 1.5 \times 10^{-5} \left(\frac{\ell}{1000}\right)^{-3} \left[1 + \left(\frac{\ell}{1000}\right)^{2.5}\right], \quad (23)$$

where $\ell_G = 1/\theta_G = 3438 (\theta_G/1 \text{ arcmin})^{-1}$.

By using Eqs. (14) and (15), one can find the following expression of $dn_{\text{peak}}/d\mathcal{K}$ in the presence of shape noise instead of Eq. (13);

$$\begin{aligned} \frac{dn_{\text{peak}}}{d\mathcal{K}} \Big|_{\mathcal{K}=\alpha} &= \int d\mathbf{D} \text{Prob}(\mathbf{D}|\mathbf{D}_{\text{cosmo}}) \int d\mathbf{D}_{\text{cosmo}} \text{Prob}(\mathbf{D}_{\text{cosmo}}) \\ &\quad \times \delta_D(\mathcal{K} - \alpha) |\det \zeta| \delta_D(\eta) \mathcal{H}(\lambda) \\ &= \int d\mathbf{D}_N \text{Prob}(\mathbf{D}_N) \int d\mathbf{D}_{\text{cosmo}} \text{Prob}(\mathbf{D}_{\text{cosmo}}) \\ &\quad \times \delta_D(\mathcal{K} - \alpha) |\det \zeta| \delta_D(\eta) \mathcal{H}(\lambda), \end{aligned} \quad (24)$$

where $\mathbf{D}_{\text{cosmo}} = \{\mathcal{K}_{\text{cosmo}}, \eta_{\text{cosmo}}, \zeta_{\text{cosmo}}\}$ and we note that $d\mathbf{D} \text{Prob}(\mathbf{D}|\mathbf{D}_{\text{cosmo}}) = d\mathbf{D}_N \text{Prob}(\mathbf{D}_N)$ where $\mathbf{D}_N = \mathbf{D} - \mathbf{D}_{\text{cosmo}}$ holds. When $\mathcal{K}_{\text{cosmo}}$ is assumed to be Gaussian random field, the number density of local maxima in \mathcal{K} field is expressed as

the following analytic formula (Bond & Efstathiou 1987):

$$\left. \frac{dn_{\text{peak}}}{d\mathcal{K}} \right|_{\mathcal{K}=\alpha} = \frac{1}{2\pi\theta_*^2} \frac{1}{\sqrt{2\pi}\sigma_0} \exp \left[-\frac{1}{2} \left(\frac{\alpha}{\sigma_0} \right)^2 \right] \times G \left(\Gamma, \Gamma \frac{\alpha}{\sigma_0} \right), \quad (25)$$

$$G(\Gamma, x_*) = (x_*^2 - \Gamma^2) \left[1 - \frac{1}{2} \operatorname{erfc} \left(\frac{x_*}{\sqrt{2(1-\Gamma^2)}} \right) \right] + \frac{x_*(1-\Gamma^2)}{\sqrt{2\pi(1-\Gamma^2)}} \exp \left(-\frac{x_*^2}{2(1-\Gamma^2)} \right) + \frac{1}{\sqrt{3-2\Gamma^2}} \exp \left(-\frac{x_*^2}{3-2\Gamma^2} \right) \left[1 - \frac{1}{2} \operatorname{erfc} \left(\frac{x_*}{\sqrt{2(1-\Gamma^2)(3-2\Gamma^2)}} \right) \right], \quad (26)$$

$$\theta_* = \frac{\sqrt{2}\sigma_1}{\sigma_2}, \quad \Gamma = \frac{\sigma_1^2}{\sigma_0\sigma_2}, \quad (27)$$

where

$$\sigma_i^2 = \int_0^\infty \frac{d^2\ell}{(2\pi)^2} \ell^{2i} |\tilde{U}(\ell)|^2 \left(\frac{\sigma_e^2}{2n_{\text{gal}}} + P_\kappa(\ell) \right). \quad (28)$$

2.3 Local-Gaussianized transformation

Assumption

In Section 2.2, we derive a general expression of the number density of local maxima in smoothed convergence field and find that the multiplicative PDF of \mathcal{K} , its first- and second-derivatives in the absence of shape noise is necessary to predict the peak counts. Here we develop a theoretical model of multiplicative PDF for cosmological convergence field $\mathcal{K}_{\text{cosmo}}$ by assuming a transformation

$$\mathcal{K}_{\text{cosmo}}(\boldsymbol{\theta}) = \mathcal{F}[y(\boldsymbol{\theta})], \quad (29)$$

where y represents a Gaussian field with unit variance¹. The functional form of \mathcal{F} is determined by the one-point PDF of $\mathcal{K}_{\text{cosmo}}$ through the following equation:

$$\int_{\mathcal{K}_{\text{cosmo}}} d\mathcal{K}'_{\text{cosmo}} \operatorname{Prob}(\mathcal{K}'_{\text{cosmo}}) = \frac{1}{2} \operatorname{erfc} \left(\frac{y}{\sqrt{2}} \right). \quad (30)$$

The statistical property of Gaussian field y is fully characterised by its power spectrum $P_y(\ell)$. When adopting Eq. (29), one expect that the two-point correlation function of y is related to that of smoothed convergence field \mathcal{K} as

$$\begin{aligned} \xi_y(\phi) &\equiv \langle y(\boldsymbol{\theta})y(\boldsymbol{\theta}+\boldsymbol{\phi}) \rangle, \\ \xi_{\mathcal{K}}(\phi) &\equiv \langle \mathcal{K}_{\text{cosmo}}(\boldsymbol{\theta})\mathcal{K}_{\text{cosmo}}(\boldsymbol{\theta}+\boldsymbol{\phi}) \rangle \\ &= \frac{1}{2\pi\sqrt{1-\xi_y(\phi)^2}} \int_{-\infty}^{\infty} du_1 \int_{-\infty}^{\infty} du_2 \\ &\quad \times \exp \left(-\frac{u_1^2}{2(1-\xi_y(\phi)^2)} \right) \exp \left(-\frac{u_2^2}{2} \right) \\ &\quad \times \mathcal{F}(u_1 + \xi_y(\phi)u_2) \mathcal{F}(u_2). \end{aligned} \quad (31)$$

Eq. (32) defines the relation between $\xi_{\mathcal{K}}$ and ξ_y . In the standard Λ CDM cosmology, the relation from Eq. (32) is found to be expressed as a monotonic function of $\xi_y = \mathcal{X}(\xi_{\mathcal{K}})$. Therefore, one

can obtain the power spectrum of y by using Fourier transform and the relation from Eq. (32) as follows

$$\begin{aligned} P_y(\ell) &= \int d^2\theta \xi_y(\theta) \exp(i\boldsymbol{\ell} \cdot \boldsymbol{\theta}) \\ &= \int d^2\theta \mathcal{X}(\xi_{\mathcal{K}}(\theta)) \exp(i\boldsymbol{\ell} \cdot \boldsymbol{\theta}), \end{aligned} \quad (33)$$

where the two-point correlation function of \mathcal{K} is defined as

$$\xi_{\mathcal{K}}(\theta) = \int \frac{d^2\ell}{(2\pi)^2} |\tilde{U}(\ell)|^2 P_{\kappa}(\ell). \quad (34)$$

Hence, for a given PDF and power spectrum of $\mathcal{K}_{\text{cosmo}}$ field, one can specify the full statistical property of a new Gaussian field y by solving Eqs. (30), (32) and (33).

Advantage and limitation

We should note the advantage and the limitation of local-Gaussianised transformation. Since the one-point PDF and the power spectrum of \mathcal{K} can be reproduced by construction, the prediction by local-Gaussianised transformation can include the appropriate information of \mathcal{K} and any order of moments $\langle \mathcal{K}^\alpha \rangle$ defined by

$$\langle \mathcal{K}^\alpha \rangle \equiv \int_{-\infty}^{\infty} d\mathcal{K}_{\text{cosmo}} \mathcal{K}_{\text{cosmo}}^\alpha \operatorname{Prob}(\mathcal{K}_{\text{cosmo}}). \quad (35)$$

Hence, the non-Gaussian information about the one-point PDF (e.g., skewness $\langle \mathcal{K}^3 \rangle$) is properly taken into account in local-Gaussianized model. Unfortunately, there is no guarantee that local-Gaussianised transformation can explain the multi-point clustering beyond power spectrum in \mathcal{K} , e.g., bispectrum. The objective of this paper is to examine if the correct information of one-point and two-point PDF of \mathcal{K} is sufficient to predict the weak-lensing peak counts. Local-Gaussianized transformation is suitable for this purpose.

Analytic expression of peak counts

From Eq. (29), one obtains

$$\begin{aligned} \eta_{\text{cosmo},i} &\equiv \nabla_i \mathcal{K}_{\text{cosmo}} = \mathcal{F}' \nabla_i y \\ &= \mathcal{F}' \eta_{y,i}, \\ \zeta_{\text{cosmo},ij} &\equiv \nabla_i \nabla_j \mathcal{K}_{\text{cosmo}} = \mathcal{F}'' (\nabla_i y)(\nabla_j y) + \mathcal{F}' \nabla_i \nabla_j y \\ &= \mathcal{F}'' \eta_{y,i} \eta_{y,j} + \mathcal{F}' \zeta_{y,ij}, \end{aligned} \quad (36)$$

where $' = d/dy$. Eqs. (36) and (37) show that the eigen values of $-\zeta_{\text{cosmo}}$ are proportional to that of $-\zeta_y$ at the position of local maxima where $\eta_{\text{cosmo}} = 0$ (i.e., $\eta_y = 0$) holds. Therefore, the expected number density of local maxima of $\mathcal{K}_{\text{cosmo}}$ under the local transformation of Eq. (29) can be derived in a similar way to Gaussian case. By using Eq. (13), one can find that

$$\begin{aligned} \left. \frac{dn_{\text{peak}}}{d\mathcal{K}_{\text{cosmo}}} \right|_{\mathcal{K}_{\text{cosmo}}=\alpha} &= \int d\mathbf{D}_{\text{cosmo}} \operatorname{Prob}(\mathbf{D}_{\text{cosmo}}) \delta_D(\mathcal{K}_{\text{cosmo}} - \alpha) \\ &\quad \times |\det \zeta_{\text{cosmo}}| \delta_D(\boldsymbol{\eta}_{\text{cosmo}}) \mathcal{H}(\boldsymbol{\lambda}_{\text{cosmo}}) \\ &= \int d\mathbf{D}_y \operatorname{Prob}(\mathbf{D}_y) \delta_D(\mathcal{F}(y) - \alpha) \\ &\quad \times |\mathcal{F}' \det \zeta_y| \delta_D(\boldsymbol{\eta}_y) \mathcal{H}(\mathcal{F}' \boldsymbol{\lambda}_y) \\ &= \frac{1}{2\pi\theta_{y*}^2} \frac{1}{\sqrt{2\pi}\sigma_{y0}} \frac{1}{\mathcal{F}'} \exp \left[-\frac{1}{2} \left(\frac{\mathcal{F}^{-1}(\alpha)}{\sigma_{y0}} \right)^2 \right] \\ &\quad \times G \left(\Gamma_y, \Gamma_y \frac{\mathcal{F}^{-1}(\alpha)}{\sigma_{y0}} \right), \end{aligned} \quad (38)$$

¹ The mean value of y can be determined by zero mean of $\mathcal{K}_{\text{cosmo}}$.

where $D_y = \{y, \eta_y, \zeta_y\}$, σ_{yi} is the i -th moment of y field, $\theta_{y*} = \sqrt{2}\sigma_{y1}/\sigma_{y2}$, $\Gamma_y = \sigma_{y1}^2/\sigma_{y0}\sigma_{y2}$, and the function of G is shown in Eq. (26).

3 NUMERICAL SIMULATION

3.1 Ray-tracing simulation

To study the weak-lensing peak count including appropriate nonlinear gravitational growth, we utilise a large set of ray-tracing simulations. The ray-tracing simulations are constructed from 200 realizations of N-body simulations with box sizes of $240 h^{-1}$ Mpc on a side. N-body simulations have been performed with the number of particles of 256^3 for the concordance Λ CDM model. In simulations, the following cosmological parameters are assumed: the matter density $\Omega_{m0} = 0.238$, the baryon density $\Omega_b = 0.042$, the dark energy density $\Omega_\Lambda = 1 - \Omega_{m0} = 0.762$, the equation of state parameters $w = -1$, the scalar spectral index $n_s = 0.958$, the amplitude of curvature perturbations $A_s = 2.35 \times 10^{-9}$ at $k = 0.002 \text{ Mpc}^{-1}$, Hubble parameter $h = 0.732$, and the variance of the present-day density fluctuation in a sphere of radius $8 h^{-1} \text{ Mpc}$ $\sigma_8 = 0.76$. We work with single source redshift at $z_{\text{source}} = 1$. From the 400 N-body simulations, we generate 1000 realizations of 5×5 sq.degs lensing convergence fields (i.e., a total of 25,000 squared degrees) with 2048^2 pixels. The angular size of each pixel is set to be 0.15 arcmin. Details of the ray-tracing simulation are found in Sato et al. (2009).

Throughout this paper, we include galaxy shape noise e in our simulation by adding to the measured shear signal random ellipticities which follow the two-dimensional Gaussian distribution as

$$P(e) = \frac{1}{\pi\sigma_{\text{sn}}^2} \exp\left(-\frac{e^2}{\sigma_{\text{sn}}^2}\right), \quad (39)$$

where $e = \sqrt{e_1^2 + e_2^2}$ and $\sigma_{\text{sn}}^2 = \sigma_e^2/(n_{\text{gal}}\theta_{\text{pix}})$ with the pixel size of $\theta_{\text{pix}} = 0.15$ arcmin. In this paper, we set $\sigma_e = 0.4$ and study two different cases of $n_{\text{gal}} = 10$ and 30 arcmin^{-1} . The former source number density corresponds to the typical value of the current-generation ground-based imaging survey, while the latter is for the future imaging surveys.

From simulated lensing shear field γ , we construct the smoothed convergence map as shown in Section 2.1 for three different smoothing scales $\theta_G = 1.2, 2.4$ and 4.8 arcmin in the absence/presence of shape noise.

3.2 Local-Gaussianized simulation

In order to specify the local-Gaussianized transformation for noiseless \mathcal{K} with a given θ_G , we measure the one-point PDF of \mathcal{K} in the absence of shape noise. We compute the PDF for 90 equally spaced bins of $(\mathcal{K} - \langle \mathcal{K} \rangle)/\sigma_{\mathcal{K}0}$ between -5 to 25 where $\sigma_{\mathcal{K}0}^2$ is the variance of \mathcal{K} without shape noise. Note that we calculate $\sigma_{\mathcal{K}0}^2$ as the average value of the variance over 1000 ray-tracing realizations. We then define the local transformation to obtain y by using averaged one-point PDF over 1000 ray-tracing realizations and Eq. (30). According to Eq. (2), the convergence field should have the minimum value which is given by

$$\kappa_{\min} = - \int_0^{\chi_{\text{source}}} d\chi W(\chi). \quad (40)$$

Nevertheless, the minimum value of smoothed field \mathcal{K} would show the dependence on θ_G and does not correspond to the value of

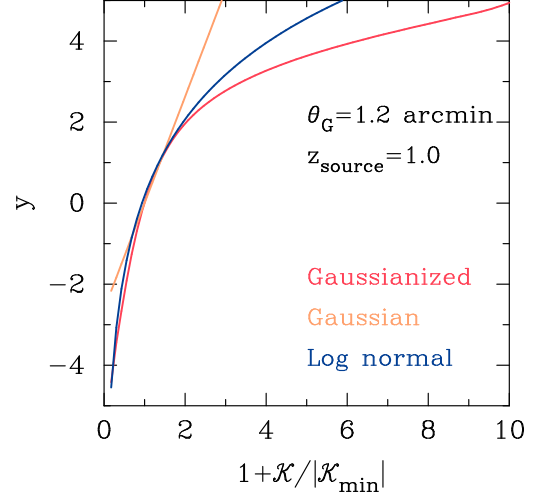


Figure 1. An example of local-Gaussianized transformation. The red line represents the relation of $\mathcal{K} = \mathcal{F}(y)$ obtained from the simulated one-point PDF in 1000 ray-tracing simulations. The yellow and blue lines show two representative examples: the yellow corresponds to the simple linear (Gaussian) relation and the blue is for the log-normal relation. In this figure, we set $\theta_G = 1.2$ arcmin.

Eq. (40) in practice. This effect would arise from the finite sampling in the limited survey area (Taruya et al. 2002). We thus simply extract the minimum \mathcal{K} from 1000 ray-tracing realizations for a given θ_G . Figure 1 shows an example of $\mathcal{K} = \mathcal{F}(y)$ obtained in our analysis for $\theta_G = 1.2$ arcmin. In this figure, we also show two representative examples as

$$1 + \frac{\mathcal{K}}{|\mathcal{K}_{\min}|} = \begin{cases} 1 + y \sigma_{\mathcal{K}0}/|\mathcal{K}_{\min}| & \text{(Gaussian)} \\ \exp(-\sigma_{\text{ln}}^2/2 + y \sigma_{\text{ln}}) & \text{(Log normal)} \end{cases}, \quad (41)$$

where \mathcal{K}_{\min} is the minimum value of simulated \mathcal{K} and $\sigma_{\text{ln}}^2 = \ln(1 + \sigma_{\mathcal{K}0}^2/|\mathcal{K}_{\min}|^2)$ (Taruya et al. 2002). Gaussian expression is a reasonable approximation for $|y| \ll 1$, while log-normal approximation can capture the feature of $\mathcal{K} > \mathcal{K}_{\min}$. For a long tail in the positive direction of \mathcal{K} , log-normal approximation is found to be insufficient and this is consistent with the conclusion of previous works (e.g., Taruya et al. 2002; Das & Ostriker 2006; Wang et al. 2009; Takahashi et al. 2011).

We also need the power spectrum of \mathcal{K} to find the power spectrum of a new Gaussian field y . We follow the method in Sato et al. (2009) to estimate the convergence power spectrum from ray-tracing simulations based on the fast Fourier transform. We measure the binned power spectrum of the (un-smoothed) convergence field by averaging the product of Fourier modes $|\tilde{\kappa}(\ell)|^2$. We employ 30 bins logarithmically spaced in the range of $\ell = 100$ to 5×10^4 . By comparing the theoretical prediction in Eq. (4) with the fitting formula of P_δ in Takahashi et al. (2012), we find that the simulated power spectrum can be approximated as

$$P_\kappa(\ell; \text{simulated}) \simeq P_\kappa(\ell; \text{theory}) \left(1.0 + \frac{\ell}{7000}\right)^{-0.21} \times \left(1.0 + \frac{\ell}{70000}\right)^{-0.12}, \quad (42)$$

where $P_\kappa(\ell; \text{simulated})$ is the average power spectrum from 1000 realizations, $P_\kappa(\ell; \text{theory})$ is the theoretical model of Eq. (4), and the correction factor represents the resolution effect in ray-tracing simulations. Since our primary focus is to construct the local transformation of Eq. (29) which can reproduce the simulated power

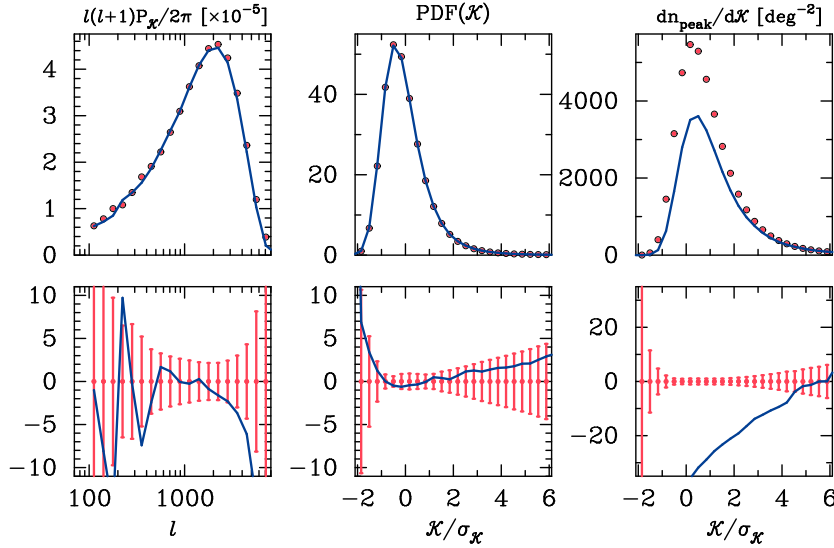


Figure 2. Comparison of different statistics in smoothed convergence field in the absence of shape noise. In each panel, the upper portion shows the comparison of a given statistical quantity measured from 1000 ray-tracing simulations and 1000 local-Gaussianized simulations, while the bottom represents the fractional difference in percentage. The red points correspond to the case of ray-tracing simulations and the blue line is for the prediction by local-Gaussianized simulations. In the bottom panels, we show the statistical uncertainty for a 1,000 squared-degrees survey, which is evaluated by the standard deviation of 1000 simulations with a survey area scaling of $1/\text{Area}$. The smoothing scale is set to be 1.2 arcmin. *Left:* The power spectrum. *Middle:* The one-point PDF. *Right:* The peak counts.

spectrum and the one-point PDF of smoothed convergence field, we work with the power spectrum approximated as in Eq. (42) to define the local-Gaussianized transformation. After some trials, we also find that by removing small- ℓ modes in Eq. (42) the variance in ray-tracing simulations is better approximated. For the input in Eq. (33), we modify the expression in Eq. (42) as

$$P_K(\ell; \text{input}) = \exp \left[- \left(\frac{2\pi}{\theta_{\text{sim}} \ell} \right)^2 \right] P_K(\ell; \text{simulated}), \quad (43)$$

where $\theta_{\text{sim}} (= 0.15 \times 2048 \times \pi / 180 / 60 \text{ rad})$ represents the field of view in ray-tracing simulations. Note that the difference between Eqs. (42) and (43) causes a $\sim 10\%$ effect in estimation of the variance of \mathcal{K} . We then define the power spectrum of y by using Eqs. (33) and (34) with the input spectrum of Eq. (43) for a given θ_G . Note that we use the fit of convergence power spectrum as in Eq. (43) not the measured power spectrum from ray-tracing simulations when computing Eqs. (33) and (34). This is because the binned spectrum from simulations is not suitable to compute the integral in Eq. (34).

When we obtain the relation of $\mathcal{K} = \mathcal{F}(y)$ and the power spectrum $P_y(\ell)$, we generate 1000 Gaussian realizations with the power spectrum of P_y and then transform a Gaussian field y into \mathcal{K} by using $\mathcal{K} = \mathcal{F}(y)$. We denote the resulting \mathcal{K} field by the local-Gaussianized transformation as \mathcal{K}_{LG} . In order to simulate the noise convergence field \mathcal{N} under the local-Gaussianized transformation, we take the following procedures:

- (i) create a random Gaussian field with zero mean and the variance of $\sigma_{\text{sn}}^2/2$
- (ii) perform smoothing with the filter of $U(\theta)$ given by Eq. (10)
- (iii) add the pixel value found in step (ii) to \mathcal{K}_{LG}

According to these procedures, we can effectively calculate the prediction of Eq. (24) by counting the local maxima in simulated $\mathcal{K}_{\text{LG}} + \mathcal{N}$ map (and thus evade the twelve-dimensional integral in Eq. (24)).

4 RESULT

In this section, we compare weak-lensing peak counts in our simulation with the prediction by local-Gaussianized transformation. By construction, the theoretical model by local-Gaussianized transformation should contain proper cosmological information in two-point clustering and any order of moments. Thus, the comparison shown here is useful to clarify how important the information of two-point clustering and moments is to predict the peak counts.

We first demonstrate how accurate the local-Gaussianized transformation can predict the one-point PDF and the power spectrum of smoothed convergence field \mathcal{K} in the absence of shape noise. In Figure 2, the left and middle panels show the comparison of the power spectrum P_K and the one-point PDF, respectively. The accuracy of local-Gaussianized model is a level of $\sim 5\%$ for P_K with the multipole of $\ell \lesssim 4,000$ and the one-point PDF with $-2 \lesssim \mathcal{K}/\sigma_{\mathcal{K}0} \lesssim 6$. On the other hand, we find that the local-Gaussianized model can *not* predict the peak count with the similar accuracy to the PDF (or $\sim 5\%$). Interestingly, the largest discrepancy between the simulated peak counts and the local-Gaussianized model is found at $\mathcal{K}/\sigma_{\mathcal{K}0} \sim 1$ where the non-Gaussianity in \mathcal{K} is expected to be smaller than the region with $\mathcal{K}/\sigma_{\mathcal{K}0} \gtrsim 5$. For high peak heights, the local-Gaussianized model is found to be a reasonable expression of simulated peak counts. It is simply because the peaks with $\mathcal{K}/\sigma_{\mathcal{K}0} \gtrsim 5$ should show a clear one-to-one correspondence to massive dark matter halos (e.g., Hamana et al. 2004; Maturi et al. 2005; Hamana et al. 2012; Shirasaki et al. 2015) and a long tail in the positive direction of \mathcal{K} is owing to such halos (e.g., Kruse & Schneider 2000). For peaks with $\mathcal{K}/\sigma_{\mathcal{K}0} \lesssim -2$, it is still difficult to obtain the converged result due to small number of peaks. Note that the minimum value of \mathcal{K} is found to be $\sim -3\sigma_{\mathcal{K}0}$ in our simulations.

Figure 3 shows the comparison of peak counts for different smoothing scales $\theta_G = 1.2, 2.4$ and 4.8 arcmin. Regardless of smoothing scales, we confirm that the local-Gaussianized

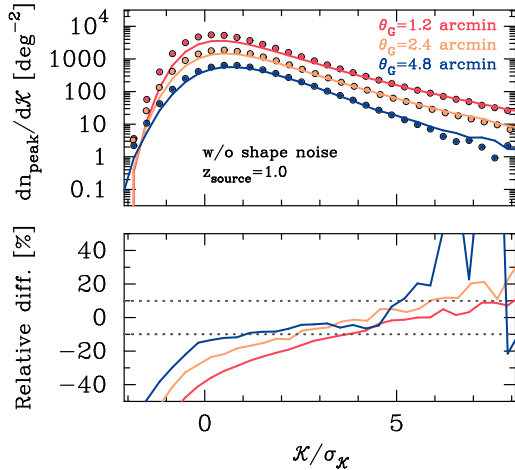


Figure 3. Comparisons of simulated peak counts with the prediction by local-Gaussianized transformation. The coloured points represent the average peak counts from 1000 ray-tracing simulations, while the lines are for the prediction by 1000 local-Gaussianized simulations. The difference of colours corresponds to the difference of smoothing scales. The top panel shows the peak count and the bottom shows the fractional differences. In this figure, we do not include the shape noise contaminants.

model can not explain the simulated peak counts in the range of $\mathcal{K}/\sigma_{\mathcal{K}0} \lesssim 3$. The discrepancy between simulated peak counts and the local-Gaussianized model tends to be smaller when one adopt larger smoothing scales. We carefully calibrate the moment of $\sigma_{\mathcal{K}i}$ and find that the local-Gaussianized model can predict $\sigma_{\mathcal{K}0}$, $\sigma_{\mathcal{K}1}$, and $\sigma_{\mathcal{K}2}$ with a few percent accuracy. Thus, the amplitude of peak counts by the local-Gaussianized model should be evaluated with the similar accuracy to the case of the one-point PDF. We also find that the positive tail in the simulated peak counts can be explained by the local-Gaussianized model quantitatively. Although peaks with extremely high height are still rare over 1000 realizations and thus require larger simulations to quantify the accuracy of local-Gaussianized model in such high \mathcal{K} regime, the local-Gaussianized model can provide a prediction of the peak counts with $\mathcal{K}/\sigma_{\mathcal{K}0} \sim 5$ with about 10% accuracy.

We next consider a more realistic case of weak-lensing peak counts by including the shape noise in ray-tracing and local-Gaussianized simulations. Figure 4 shows the comparison of peak counts in the presence of shape noise. As a reference, the dashed lines represent the Gaussian prediction of peak counts as in Eq. (25).

In the case of the source number density of $n_{\text{gal}} = 10 \text{ arcmin}^{-2}$ corresponding to the typical value in the current lensing surveys (e.g., Erben et al. 2013), the local-Gaussianized model can predict the simulated peak counts in the range of $-1 \lesssim \mathcal{K}/\sigma_{\mathcal{K}0} \lesssim 4$ with a $\sim 10\%$ accuracy, while the Gaussian prediction is also found to work within a 10% accuracy for $|\mathcal{K}|/\sigma_{\mathcal{K}0} \lesssim 1$. Note that the current lensing surveys already require a prediction of peak counts with an accuracy level of $\sim 10\%$ (e.g., Liu et al. 2015a). The non-Gaussian tail in simulated peak counts can be also explained by the local-Gaussianized model quantitatively even in this realistic case.

When we increase the source number density of $n_{\text{gal}} = 30 \text{ arcmin}^{-2}$, the Gaussian prediction can not provide an explanation of simulated peak counts even in $|\mathcal{K}|/\sigma_{\mathcal{K}0} \lesssim 1$, while the local-Gaussianized model can still explain the simulated peak counts with a $\sim 10\%$ accuracy in the range of $-1 \lesssim \mathcal{K}/\sigma_{\mathcal{K}0} \lesssim 4$.

According to Figure 4, the simulated peak counts would surely contain the cosmological information of higher-order moments beyond variance such as skewness even in the presence of shape noise. Although the local-Gaussianized model can explain the simulated peak counts better than the Gaussian prediction, there still remains room for improvement on theoretical model of weak-lensing peak counts, except for including the appropriate information of higher-order moments than variance such as skewness.

5 CONCLUSION AND DISCUSSION

We aimed at studying the cosmological information in the number density of local maxima of weak lensing field or weak-lensing peak counts. In particular, we have considered the statistical connection to peak counts with two-point clustering and moments in weak lensing field. We first have developed a statistical model of smoothed convergence field \mathcal{K} assumed to be related with a new Gaussian field y . We refer the relation between \mathcal{K} and y as local-Gaussianized transformation. Our model has been calibrated with 1000 ray-tracing simulations so that the one-point PDF and the power spectrum of \mathcal{K} can be reproduced with a $\lesssim 5\%$ accuracy. Therefore, local-Gaussianized transformation should contain the cosmological information of the power spectrum and moments as similar to the simulated \mathcal{K} field. By comparing the simulated peak counts and the local-Gaussianized prediction, we can assess whether the accurate modeling of two-point clustering and any order of moments is sufficient to predict the peak counts in \mathcal{K} field.

We found that the local-Gaussianized transformation is unable to predict the simulated peak counts in the absence of shape noise and the differences between two are $\sim 30\%$ over a wide range of peak heights for various smoothing scales. Interestingly, the differences are more prominent for peaks with the height of $\sim 1 - 2 \sigma_{\mathcal{K}0}$ where $\sigma_{\mathcal{K}0}^2$ represents the variance of \mathcal{K} field. These results imply that it is necessary to include other information beyond two-point clustering and moments in theoretical model of peak counts for the first time. Also, we studied the effect of shape noise on weak-lensing peak counts and found that the local-Gaussianized model can provide more reasonable explanation for simulated peak counts than the Gaussian prediction. The local-Gaussianized model can achieve a $\sim 10\%$ accuracy of weak-lensing peak counts in the presence of shape noise, whereas the upcoming lensing surveys would require the statistical uncertainty of a few percent or less. Hence, we conclude that weak-lensing peak counts include the cosmological information of higher-order moments than second-order one even in the presence of shape noise with a realistic level, while including the higher-order moments like skewness is not complete to predict the simulated peak count with the desired accuracy for future surveys. This is consistent with previous theoretical works on the inadequacy of multiple-point correlation functions to describe nonlinear cosmological fields (e.g., Carron 2012; Carron & Neyrinck 2012). Our conclusion is also in good agreement with previous lensing studies showing the moments of the convergence field and of its spatial derivatives do not contain all the information in the maps (Petri et al. 2013, 2015). We note that the medium peak contain rich cosmological information even in the presence of shape noise (Kratochvil et al. 2010).

We have shown that the local-Gaussianized transformation can explain the non-Gaussian tail in the simulated peak counts quantitatively. As expected, peaks with a significantly positive height are originated from individual massive dark matter halos along the line of sight. Such massive halos can also produce a long

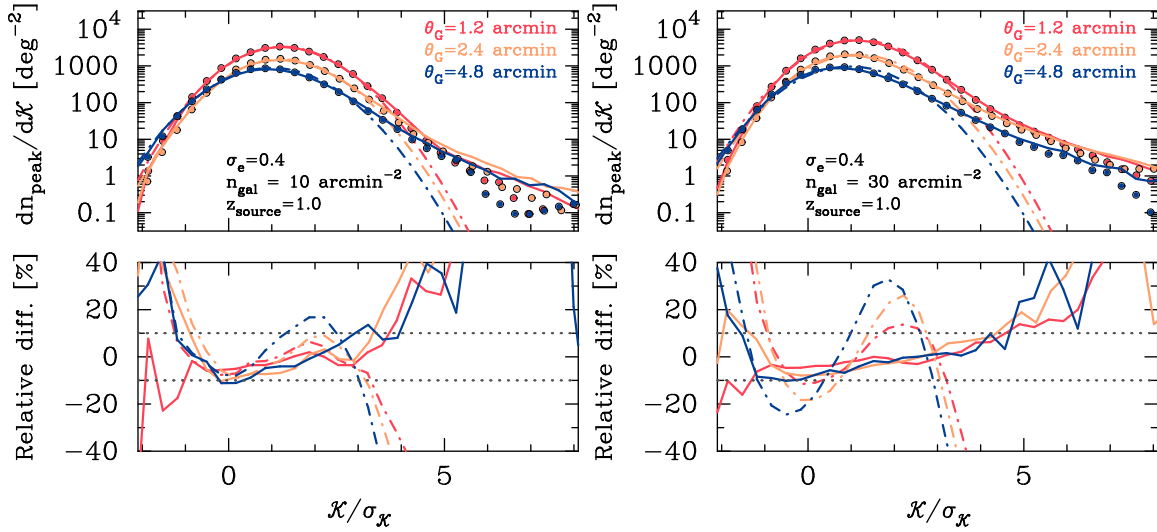


Figure 4. Similar to Figure 3, but the shape noise are taken into account. The left panels summarise the result with the source number density of $n_{\text{gal}} = 10 \text{ arcmin}^{-2}$, while the right is for $n_{\text{gal}} = 30 \text{ arcmin}^{-2}$. Note that coloured dashed lines represent the Gaussian prediction for different smoothing scales.

tail in the positive direction of \mathcal{K} in the one-point PDF. Therefore, in high \mathcal{K} regime, the local mapping $\mathcal{K}(\theta)$ to a Gaussian field $y(\theta)$ is a reasonable approximation. On the other hand, the local mapping does not accurately reproduce medium peaks with the height of $\lesssim 1 - 2\sigma_{\mathcal{K}0}$ because previous works have shown such peaks might be induced by the superposition of massive dark matter halos along the line of sight (e.g., Yang et al. 2011; Liu & Haiman 2016). Obviously, the smoothing procedure would also make the local mapping $\mathcal{K}(\theta) \mapsto y(\theta)$ invalid. Thus, a non-local relation between \mathcal{K} and a Gaussian field y would be needed. Nonlocality should, by definition, include the information of multiple-point clustering in cosmological \mathcal{K} field. In the appendix, we demonstrate the importance of including the information on correlation between Fourier modes in modeling of weak-lensing peak counts.

The numerical study in this paper is the first step to clarify the cosmological information of weak-lensing peak counts and its relation to other statistics. Although accurate theoretical model of peak counts needs to be further developed, our analysis proved that peak counts should contain the cosmological information of two-point clustering, any order of moments, and *others* in weak lensing field.

ACKNOWLEDGMENTS

The author thanks an anonymous referee for careful reading and suggestion to improve the article. The author would like to thank Naoki Yoshida for helpful discussions and comments on the manuscript. The author appreciates the helpful comments of Jia Liu, Takashi Hamana, and Zoltan Haiman. The author is supported by Research Fellowships of the Japan Society for the Promotion of Science (JSPS) for Young Scientists. Numerical computations presented in this paper were in part carried out on the general-purpose PC farm at Center for Computational Astrophysics, CfCA, of National Astronomical Observatory of Japan.

REFERENCES

Anderson L., et al., 2012, *MNRAS*, **427**, 3435

- Bard D., et al., 2013, *ApJ*, **774**, 49
 Bardeen J. M., Bond J. R., Kaiser N., Szalay A. S., 1986, *ApJ*, **304**, 15
 Bartelmann M., Schneider P., 2001, *Physical Rep.*, **340**, 291
 Becker M. R., et al., 2016, *Phys. Rev.*, **D94**, 022002
 Bond J. R., Efstathiou G., 1987, *MNRAS*, **226**, 655
 Carron J., 2012, *Physical Review Letters*, **108**, 071301
 Carron J., Neyrinck M. C., 2012, *ApJ*, **750**, 28
 Chang C., et al., 2015, *Physical Review Letters*, **115**, 051301
 Das S., Ostriker J. P., 2006, *ApJ*, **645**, 1
 Dietrich J. P., Hartlap J., 2010, *MNRAS*, **402**, 1049
 Erben T., et al., 2013, *MNRAS*, **433**, 2545
 Hamana T., Takada M., Yoshida N., 2004, *MNRAS*, **350**, 893
 Hamana T., Oguri M., Shirasaki M., Sato M., 2012, *MNRAS*, **425**, 2287
 Hamana T., Sakurai J., Koike M., Miller L., 2015, *PASJ*, **67**, 34
 Hennawi J. F., Spergel D. N., 2005, *ApJ*, **624**, 59
 Hilbert S., Marian L., Smith R. E., Desjacques V., 2012, *MNRAS*, **426**, 2870
 Huterer D., 2010, *General Relativity and Gravitation*, **42**, 2177
 Kacprzak T., et al., 2016, *MNRAS*, **463**, 3653
 Kaiser N., 1992, *ApJ*, **388**, 272
 Kilbinger M., 2015, *Reports on Progress in Physics*, **78**, 086901
 Kratochvil J. M., Haiman Z., May M., 2010, *Phys. Rev. D*, **81**, 043519
 Kruse G., Schneider P., 2000, *MNRAS*, **318**, 321
 Lilje P. B., 1992, *ApJ*, **386**, L33
 Limber D. N., 1954, *ApJ*, **119**, 655
 Lin C.-A., Kilbinger M., 2015, *A&A*, **576**, A24
 Liu J., Haiman Z., 2016, *Phys. Rev. D*, **94**, 043533
 Liu J., Petri A., Haiman Z., Hui L., Kratochvil J. M., May M., 2015a, *Phys. Rev. D*, **91**, 063507
 Liu X., et al., 2015b, *MNRAS*, **450**, 2888
 Liu X., et al., 2016, *Physical Review Letters*, **117**, 051101
 Marian L., Bernstein G. M., 2006, *Phys. Rev. D*, **73**, 123525
 Marian L., Hilbert S., Smith R. E., Schneider P., Desjacques V., 2011, *ApJ*, **728**, L13
 Marian L., Smith R. E., Hilbert S., Schneider P., 2012, *MNRAS*, **423**, 1711
 Massey R., et al., 2007, *Nature*, **445**, 286
 Matsubara T., 2003, *ApJ*, **591**, L79
 Matsubara T., 2007, *ApJS*, **170**, 1
 Maturi M., Meneghetti M., Bartelmann M., Dolag K., Moscardini L., 2005, *A&A*, **442**, 851
 Miyazaki S., Hamana T., Ellis R. S., Kashikawa N., Massey R. J., Taylor J., Refregier A., 2007, *ApJ*, **669**, 714
 Miyazaki S., et al., 2015, *ApJ*, **807**, 22

- Osato K., Shirasaki M., Yoshida N., 2015, *ApJ*, **806**, 186
- Pen U.-L., Zhang T., van Waerbeke L., Mellier Y., Zhang P., Dubinski J., 2003, *ApJ*, **592**, 664
- Petri A., Haiman Z., Hui L., May M., Kratochvil J. M., 2013, *Phys. Rev. D*, **88**, 123002
- Petri A., Liu J., Haiman Z., May M., Hui L., Kratochvil J. M., 2015, *Phys. Rev. D*, **91**, 103511
- Planck Collaboration et al., 2015, arXiv:1507.02704,
- Sato M., Hamana T., Takahashi R., Takada M., Yoshida N., Matsubara T., Sugiyama N., 2009, *ApJ*, **701**, 945
- Schirmer M., Erben T., Hettterscheidt M., Schneider P., 2007, *A&A*, **462**, 875
- Schneider P., 1996, *MNRAS*, **283**, 837
- Shan H., et al., 2012, *ApJ*, **748**, 56
- Shirasaki M., Hamana T., Yoshida N., 2015, *MNRAS*, **453**, 3043
- Shirasaki M., Hamana T., Yoshida N., 2016, *PASJ*, **68**, 4
- Takahashi R., Oguri M., Sato M., Hamana T., 2011, *ApJ*, **742**, 15
- Takahashi R., Sato M., Nishimichi T., Taruya A., Oguri M., 2012, *ApJ*, **761**, 152
- Taruya A., Takada M., Hamana T., Kayo I., Futamase T., 2002, *ApJ*, **571**, 638
- Van Waerbeke L., et al., 2013, *MNRAS*, **433**, 3373
- Wang S., Haiman Z., May M., 2009, *ApJ*, **691**, 547
- Yang X., Kratochvil J. M., Wang S., Lim E. A., Haiman Z., May M., 2011, *Phys. Rev. D*, **84**, 043529
- Yang X., Kratochvil J. M., Huffenberger K., Haiman Z., May M., 2013, *Phys. Rev. D*, **87**, 023511
- Yu Y., Zhang P., Jing Y., 2016, arXiv:1607.05007,
- Zorrilla Matilla J. M., Haiman Z., Hsu D., Gupta A., Petri A., 2016, arXiv:1609.03973,
- van Waerbeke L., 2000, *MNRAS*, **313**, 524

APPENDIX A: MISSING INFORMATION IN LOCAL-GAUSSIANIZED TRANSFORMATION FOR MODELING OF WEAK-LENSING PEAK COUNTS

In this appendix, we examine if weak-lensing peak counts can be reproduced by including the correct information of Fourier-mode distribution. We consider the inverse transformation of Eq. (29) and apply it to 1000 ray-tracing simulations in order to obtain its counter-part of Gaussian field y :

$$y_{\text{RT}}(\boldsymbol{\theta}) = \mathcal{F}^{-1}(\mathcal{K}_{\text{RT}}(\boldsymbol{\theta})), \quad (\text{A1})$$

where \mathcal{K}_{RT} represents the smoothed convergence field obtained from ray-tracing simulation. Under the local transformation of Eq. (29), the statistical information of \mathcal{K} field in ray-tracing simulations should be preserved in that of y_{RT} . The full statistical information of y_{RT} can be characterised by the distribution in Fourier mode $y_{\text{RT},\ell}$. In general, the distribution of Fourier mode A_ℓ is expressed as the function of norm $|A_\ell|$ and phase $\theta_{A,\ell}$. For a Gaussian field, the distribution of A_ℓ is given by

$$\text{Prob}(|A_\ell|, \theta_{A,\ell}) \equiv \mathcal{P}_G(|A_\ell|) \mathcal{P}_G(\theta_{A,\ell}), \quad (\text{A2})$$

$$\begin{aligned} \mathcal{P}_G(|A_\ell|) &= \frac{2}{\sqrt{P_A(\ell)}} \left(\frac{|A_\ell|}{\sqrt{P_A(\ell)}} \right) \\ &\times \exp \left[- \left(\frac{|A_\ell|}{\sqrt{P_A(\ell)}} \right)^2 \right], \end{aligned} \quad (\text{A3})$$

$$\mathcal{P}_G(\theta_{A,\ell}) = \frac{1}{2\pi}, \quad (\text{A4})$$

where $P_A(\ell)$ is the power spectrum of A . For a weakly non-Gaussian field, the perturbative approaches have been developed

(Matsubara 2003, 2007) and the lowest-order non-Gaussian effect in $\text{Prob}(|A_\ell|, \theta_{A,\ell})$ is related to the three-point correlation in Fourier space, or Bispectrum. Also, the correlation between norm $|A_\ell|$ and phase $\theta_{A,\ell}$ are naturally induced in the non-Gaussian field.

In our local-Gaussianized model, we distribute the Fourier mode of y with Eq. (A2). Here we extend the model in two different ways by directly using the distribution of $y_{\text{RT},\ell}$ constructed from ray-tracing simulations. In the first model, we keep the distribution of $|y_\ell|$ as in Gaussian with Eq. (A3) but include the phase correlation with the distribution of $\theta_{y_{\text{RT},\ell}}$. We denote this as phase-shared model. In the phase-shared model, we realise the similar morphology in \mathcal{K} to a given ray-tracing map \mathcal{K}_{RT} since we use the same distribution of the Fourier phase as ray-tracing simulations. In the second model, we distribute the Fourier phase of y randomly as in Eq. (A4), while we use the simulated distribution of $|y_{\text{RT},\ell}|$ instead of Eq. (A3). We denote this model as norm-shared model. In phase- and norm-shared models, we include the multiple-point correlations of Fourier-mode phase and norm, respectively. Although we can include any order of multiple-point correlations of phases (norm) in phase-shared (norm-shared) models, we ignore the correlation between the Fourier-mode phase and norm. For both phase- and norm-shared models, we generate 1000 realizations of y field and then convert y into \mathcal{K} with Eq. (29).

Figure A1 shows the comparison of peak counts among the different models. The red points represent the simulated peak counts measured in 1000 ray-tracing simulations. The blue, yellow and cyan lines correspond to the local-Gaussianized model, the phase-shared model and the norm-shared model, respectively. In this figure, we ignore the shape noise contaminants and set the smoothing scale to be 1.2 arcmin. We find that the phase correlation does not improve the model prediction by local-Gaussianised transformation. The effect of the phase correlation on peak counts is found to be $\lesssim 1\%$. This indicates that the correct morphological information in \mathcal{K} would be of little importance to predict the weak-lensing peak counts. We also find that the information of multiple-point correlation of the Fourier-mode norm significantly increases the number of peaks over a wide range of peak heights by a factor of 3 – 5, while the variance of \mathcal{K} in the norm-shared model is found to be consistent with full ray-tracing simulations with a level of $\sim 30\%$. Also, the difference between the norm-shared model and the ray-tracing result depends on peak height, showing that a simple correction by scaling of the overall amplitude of peak counts can not work.

Hence, the difference of weak-lensing peak counts between ray-tracing simulations and our local-Gaussianised model are caused by the distribution of y_{RT} in Fourier space. In particular, the phase correlation in \mathcal{K} would be minor, while the correlation between the Fourier-mode norm $|y_\ell|$ and phase $\theta_{y,\ell}$ should play a central role to determine the cosmological information of weak-lensing peak counts.

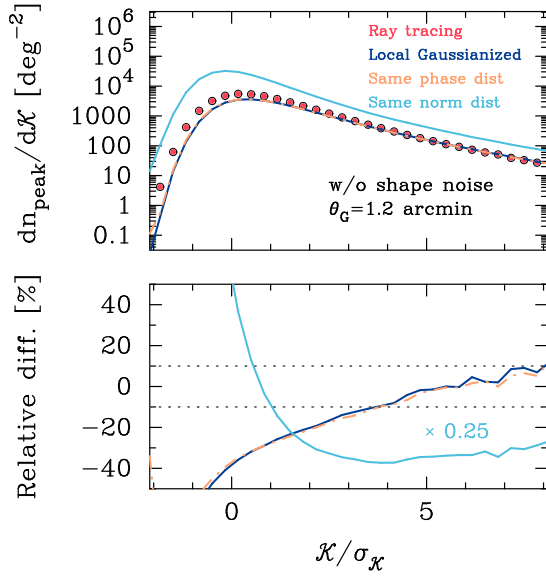


Figure A1. Connection of weak-lensing peak counts with the Fourier-mode statistics. Figure representation is similar to Figure 3. The red points represent the average peak counts over 1000 ray-tracing simulations. The different coloured lines correspond to the theoretical models based on a local transformation of lensing field \mathcal{K} to a new field y . The local relation between \mathcal{K} and y is defined by Eq. (30), while the statistical property of y field in Fourier space is different among them. The blue line is our baseline model assumed that y follows Gaussian. The yellow line is similar to the blue one but takes into account the phase correlation, while the cyan line shows a model with the correct distribution of the amplitude of Fourier mode $|y_{\ell}|$ and the random phase. The details are found in the text. In the bottom panel, we scale the cyan line by a factor of 0.25 for illustrative purpose.